Journal of Materials Chemistry C

Materials for optical and electronic devices

www.rsc.org/MaterialsC

Volume 1 | Number 23 | 21 June 2013 | Pages 3625–3748

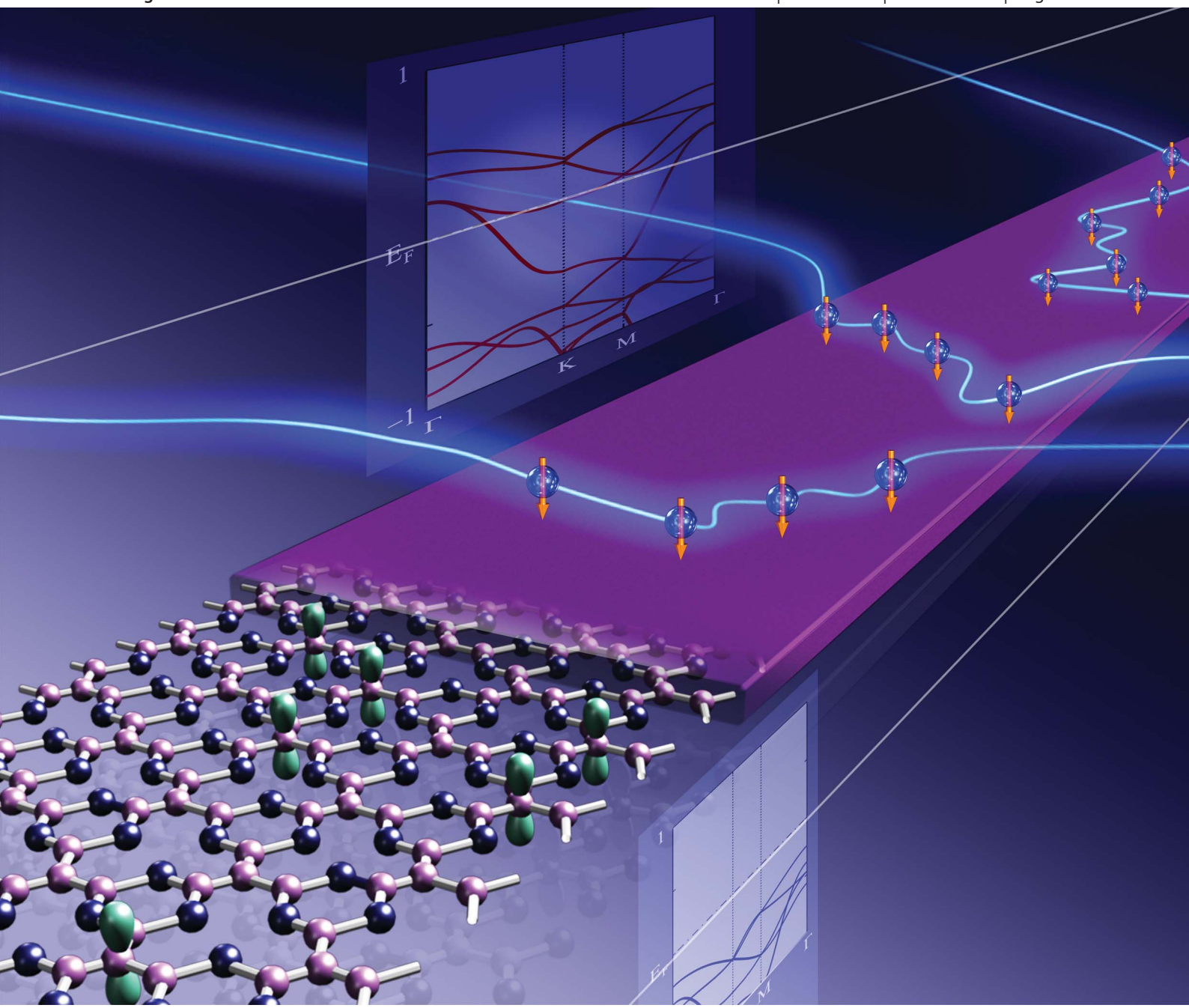

ISSN 2050-7526

RSC Publishing

PAPER

Shimin Hou *et al.*

Origin of the half-metallic properties of graphitic carbon nitride in bulk and confined forms

2050-7526(2013)1:23;1-G

Journal of Materials Chemistry C

RSC Publishing

PAPER

View Article Online
View Journal | View Issue

Origin of the half-metallic properties of graphitic carbon nitride in bulk and confined forms†

Cite this: *J. Mater. Chem. C*, 2013, **1**, 3655

Yang Li,[a] Stefano Sanvito[b] and Shimin Hou*[a]

The electronic and magnetic properties of graphitic carbon nitride (g-C_4N_3) in both its bulk and confined form are investigated by using density functional theory. Our calculations show that the $2p_z$ orbital of the carbon atoms connecting the *sym*-triazine structure units plays a decisive role in the half-metallic character of these materials. In the bulk two-dimensional (2D) case, the $2p_z$ orbital of the connecting carbon atom couples weakly with the frontier molecular orbitals of the *sym*-triazine ring due to symmetry mismatch and a large energy separation. As a consequence a narrow energy band is formed near the Fermi level. This spin splits in virtue of the Stoner criterion and thereby gives rise to spin polarization in the (1×1) primitive cell. Such a magnetic state is not destroyed by a (2×2) reconstruction, which further enhances the half-metallic character of the 2D g-C_4N_3 sheet. When the dimension is reduced, size and edge effects become dominant. Both zigzag and armchair one-dimensional g-C_4N_3 nanoribbons with H-terminated edges preserve the half-metallicity, at least down to a critical ribbon width. Furthermore, the electronic and magnetic properties of these g-C_4N_3 nanoribbons can be tuned by controlling the π-type coupling between the passivating functional groups and the $2p_z$ orbital of the connecting carbon atoms at the ribbon edges, demonstrating that g-C_4N_3 may be an interesting material platform for applications in future spintronic devices.

Received 27th February 2013
Accepted 11th April 2013

DOI: 10.1039/c3tc30371c

www.rsc.org/MaterialsC

1 Introduction

Half-metallic magnets, which display a metallic density of states (DOS) for one spin component but are insulating or semiconducting for the other, have promising applications in spintronic devices as spin filters and spin injectors.[1,2] Thus, much research effort has been devoted to the search for novel materials with robust half-metallic properties. When compared to transition-metal-containing compounds, such as manganese perovskites,[3] Heusler alloys[4] and dilute magnetic semiconductors,[5] half-metallic graphene-based materials appear more attractive because of the long spin coherence length in carbon and their compatibility with the maturing graphene technological area.[6,7] Although a half-metallic DOS has been predicted for zigzag graphene nanoribbons in the presence of an electric field or when their edges are modified by appropriate organic functional groups,[8,9] the prohibitively large electric field and the fine control of the positions of functional groups make the experimental synthesis of these materials highly improbable.

Recently one intriguing functional carbon material with an extended framework has been synthesized by trimerization of a nitrile-containing anion.[10] This can be considered as a *sym*-triazine structural unit connected by carbon atoms. Such a new type of two-dimensional (2D) graphitic carbon nitride (g-C_4N_3) material has been predicted to possess an intrinsic half-metallicity by first-principles calculations.[11] It was found that the ground state of the primitive (1×1) g-C_4N_3 cell is spin-polarized with a magnetic moment of 1 μ_B per unit cell and that the (2×2) reconstruction further enhances its half-metallic characteristics. Clearly, the magnetism of g-C_4N_3 does not originate from d or f electrons, thus it is quite interesting to explore what is the driving force for the occurrence of spin polarization in this sp-material.

Furthermore, for practical applications this functional material must be cut into ribbons, where finite-size effects and edge related features might dominate the low energy electronic structure and significantly influence the half-metallicity. Therefore, in order to address these important issues we perform density functional theory (DFT) calculations for the g-C_4N_3 2D sheet, one-dimensional (1D) nanoribbons and zero-dimensional (0D) nanodots. Our calculations show that the $2p_z$ orbital of the connecting carbon atoms plays an important role in the half-metallic characteristics. In the case of 2D g-C_4N_3, such $2p_z$ orbital forms a narrow energy band due to its weak coupling to the frontier molecular orbitals of the *sym*-triazine ring and thus results in a high DOS near the Fermi level. This is electronically unstable and results in a spin polarization of the (1×1) primitive cell, according to the Stoner criterion, which is

[a]*Centre for Nanoscale Science and Technology, Key Laboratory for the Physics and Chemistry of Nanodevices, Department of Electronics, Peking University, Beijing 100871, China. E-mail: smhou@pku.edu.cn*

[b]*School of Physics and CRANN, Trinity College, Dublin 2, Ireland*

† Electronic supplementary information (ESI) available. See DOI: 10.1039/c3tc30371c

enhanced by the (2 × 2) reconstruction. In contrast, for 1D g-C_4N_3 nanoribbons we find that in order to maintain the half-metallicity not only must the ribbon widths be larger than a critical value (about 2 nm for zigzag and about 3 nm for armchair nanoribbons), but also π-type perturbations of the $2p_z$ orbital of the connecting carbon atom at the ribbon edges should be avoided.

2 Calculation method

For the calculation of the electronic properties of bulk 2D g-C_4N_3 and 1D g-C_4N_3 nanoribbons, the SIESTA package is adopted.[12] We consider improved Troullier–Martins pseudopotentials to describe the core electrons while a numerical basis set of double-ζ polarized quality expands the wave functions of the valence electrons.[13] The generalized gradient approximation (GGA) in the Perdew–Burke–Ernzerhof (PBE) form is used to account for electron–electron interactions.[14] Geometry optimization is obtained by conjugate gradient relaxation until the forces are smaller than 0.02 eV $Å^{-1}$. In order to model isolated 2D g-C_4N_3 sheets and 1D g-C_4N_3 nanoribbons, the perpendicular distance between the neighboring g-C_4N_3 cells is set to be 30 Å. For 1D g-C_4N_3 nanoribbons an additional vacuum layer 18 Å thick is also inserted in the in-plane direction. In contrast, for the calculation of the isolated *sym*-triazine molecule and for 0D g-C_4N_3 nanodots the GAUSSIAN 03 code is employed.[15] The GGA-PBE functional is also used together with an all-electron 6-311+G(d,p) basis set.[16]

3 Results and discussion

sym-Triazine molecule in the gas phase

Since the *sym*-triazine unit is the basic building block for g-C_4N_3 materials, we investigate first the atomic and electronic structures of an isolated *sym*-triazine molecule. As shown in Fig. 1(a), at the PBEPBE/6-311+G(d,p) level *sym*-triazine in the gas phase is optimized to be a planar six-member ring with a C–N bond length of 1.343 Å, in good agreement with the experimental value (1.338 Å).[17] Similar results are also obtained using SIESTA, and the differences in the calculated C–N and C–H bond lengths between these two methods are less than 0.01 Å, confirming the appropriateness of the pseudopotentials and basis functions for the C, N and H atoms built for this work. Although the atomic structure of *sym*-triazine is very similar to that of benzene, their corresponding electronic structures are significantly different, especially concerning the occupied molecular orbitals (see ESI Fig. S1†). It is well-known that the highest occupied molecular orbital (HOMO) of benzene is a doubly degenerate π-type orbital composed of the carbon $2p_z$ atomic orbital. In contrast, due to the large difference between the electronegativities of C and N, the *sym*-triazine HOMO is a doubly degenerate orbital of σ-type symmetry and is dominated by the nitrogen sp^2 hybrid orbitals accommodating their lone pairs. In this case the doubly degenerate π-type orbital with the same symmetry as the benzene HOMO is shifted downward in energy and becomes the *sym*-triazine HOMO − 1. When the unoccupied molecular orbitals are considered, the difference between *sym*-triazine and benzene is not so evident since both have a doubly degenerate π-type lowest unoccupied molecular orbital (LUMO) with the same symmetry. Finally, the HOMO–LUMO GGA-calculated gap of the *sym*-triazine molecule is 3.82 eV, *i.e.* it is about 1.3 eV smaller than that of benzene (5.08 eV) calculated at the same level.

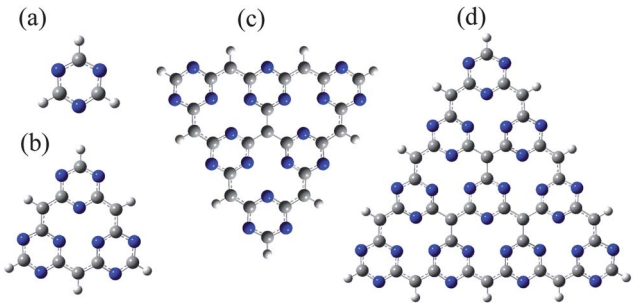

Fig. 1 Optimized atomic structures of the isolated *sym*-triazine molecule and various 0D g-C_4N_3 nanodots.

0D g-C_4N_3 nanodots

Then we move to investigate the atomic and electronic structures of g-C_4N_3 nanodots, which are composed of *sym*-triazine rings connected by carbon atoms. In the three g-C_4N_3 nanodots investigated here (Fig. 1), the *sym*-triazine rings are arranged in a triangle configuration, and the numbers of *sym*-triazine rings are respectively 3, 6 and 10, while the numbers of connecting C are correspondingly 3, 7 and 12. Depending on their positions, the connecting carbon atoms can be classified into two categories: (i) the C atoms at the periphery which are connected with two *sym*-triazine rings and thus one hydrogen atom is employed to passivate the remaining dangling bond and (ii) the C atoms in the interior of the dot which are coordinated with three neighboring *sym*-triazine rings and thus no dangling bonds exist. At variance with the isolated *sym*-triazine molecule, which has a spin-degenerate ground state, these three g-C_4N_3 nanodots are all spin-polarized and their magnetic moments are calculated to be 3.0 μ_B, 7.0 μ_B and 12.0 μ_B respectively, *i.e.* there is 1.0 μ_B for each connecting carbon atom. Although the atoms in these three g-C_4N_3 nanodots are not located in the same plane, the sp^2 hybridization is maintained since the local chemical structure of each atom is very close to the ideal sp^2 case. For example, the bond angles of C(*sym*-triazine)–C(connecting)–C(*sym*-triazine) and C(*sym*-triazine)–C(connecting)–H in the g-C_4N_3 nanodot composed of three *sym*-triazine rings (Fig. 1(b)) are optimized respectively to be 122.94° and 118.07°, slightly different from the ideal value of 120°. Since the number of unpaired electrons in these g-C_4N_3 nanodots is just equal to that of the connecting carbon atoms, we can infer that the electronic and magnetic properties of g-C_4N_3 nanodots are dominated by the interaction among the $2p_z$ electrons of the connecting carbon atoms and that their spins prefer coupling ferromagnetically in the ground state. A ferromagnetic coupling between the spins of the $2p_z$ electrons of the connecting carbon atoms lowers the total energy of these g-C_4N_3 nanodots, because their orbital overlap is small and their exchange energy is negative. This will become clearer in the following discussions

Table 1 The HOMO–LUMO gap of 0D g-C_4N_3 nanodots of different sizes

Nanodots	HOMO–LUMO gap for α electrons (eV)	HOMO–LUMO gap for β electrons (eV)
sym-Triazine	3.82	3.82
Dot 1	2.90	0.36
Dot 2	2.76	0.28
Dot 3	2.70	0.20

about 2D bulk g-C_4N_3. As listed in Table 1, the HOMO–LUMO gap is always very large for the α electrons (more than 2.5 eV), but small for the β electrons (less than 0.4 eV). Here α and β electrons refer to spin-up and spin-down electrons, respectively. Following the increase of the dot size, the HOMO–LUMO gap for the β electrons also decreases rather quickly. Thus, one can expect that, when the nanodot is large enough, its HOMO–LUMO gap for the β electrons will disappear while its HOMO–LUMO gap for the α electrons will still keep a finite value.

2D bulk g-C_4N_3

Now we are ready to investigate the origin of spin polarization in 2D bulk g-C_4N_3. As shown in Fig. 2(a), when the calculation is performed without allowing for spin polarization the primitive (1×1) g-C_4N_3 cell has a metallic ground state with three energy bands crossing the Fermi level, E_F. In particular, two of the energy bands are narrow and generate a high DOS around E_F, which is characterized by a sharp DOS peak centered at −0.25 eV together with a small shoulder at a slightly higher energy. This electronic structure suggests instability of the primitive (1×1) g-C_4N_3 cell against spin polarization, in virtue of the Stoner criterion. Projecting the DOS onto the C and N atomic orbitals shows that the sharp DOS peak at −0.25 eV is mainly contributed by the $2p_z$ orbitals of the connecting C and the three N atoms in the *sym*-triazine ring and that the small shoulder is dominated by the N $2p_x$, $2p_y$ and 2s orbitals. These latter orbitals also contribute to the flat DOS extending from 0.35 eV above E_F to 2.72 eV below E_F and correspond to the dispersive energy band around the Fermi level. Such a low-energy electronic structure is very different from that of graphene in which the energy bands around the Fermi level are entirely due to the carbon $2p_z$ atomic orbital.

The peculiar non-spin-polarized electronic structure of the primitive (1×1) g-C_4N_3 cell can be rationalized by considering the interaction between the *sym*-triazine ring and the connecting C atom. Since the HOMO of the *sym*-triazine molecule is σ-type in nature, symmetry does not allow it to electronically couple to the $2p_z$ orbital of the connecting carbon atom. In addition, although the HOMO − 1 and the LUMO of the *sym*-triazine molecule are both π-type, their coupling with the $2p_z$ orbital of the connecting carbon atom is rather weak due to the large energy separation. Thus, the $2p_z$ orbital of the connecting carbon atom forms a very narrow energy band across E_F and favors spin-polarization. This is indeed the case and in fact the total energy of the primitive (1×1) g-C_4N_3 is lowered by about 96 meV, when spin-polarization is allowed in the calculation. It should be noted that the energy bands contributed by the $2p_z$ orbital of the connecting carbon atom are just below E_F for both spin-up and spin-down electrons, whereas the two energy bands dominated by the N $2p_x$ and $2p_y$ atomic orbitals are shifted well above the Fermi level for the spin-down electrons (Fig. 2(b)). Thus, spin density is more clearly seen in the nitrogen $2p_x$ and $2p_y$ atomic orbitals. Furthermore, the (2×2) reconstruction of the g-C_4N_3 sheet not only enhances its half-metallic properties but also makes visible the spin profile contributed by the $2p_z$ orbital of the connecting carbon atom.[11]

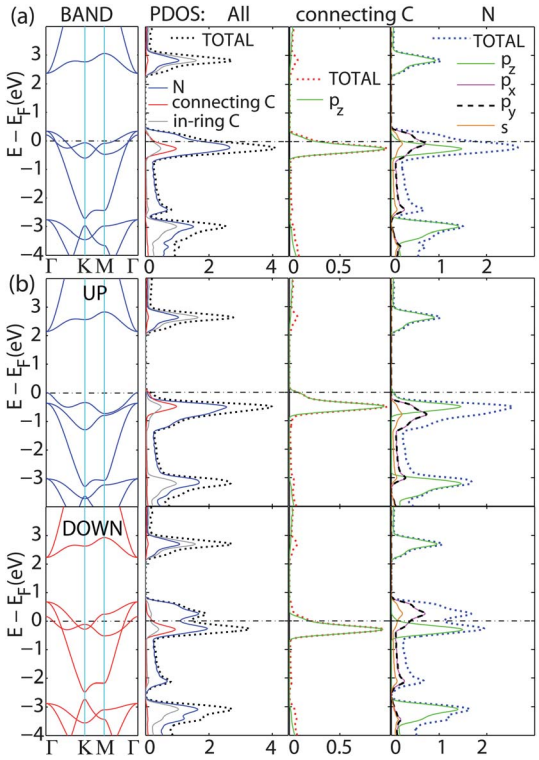

Fig. 2 Band structure and DOS of the primitive (1×1) g-C_4N_3 cell for (a) the non-spin-polarized and (b) the spin-polarized case. The DOS is also projected (PDOS) over the C and N atoms in the *sym*-triazine unit and over the C atom connecting the *sym*-triazine units (second panel from the left). Furthermore for the connecting C and N atoms we provide the orbital-resolved DOS (respectively the third and fourth panels from the left).

The instability of the primitive (1×1) g-C_4N_3 cell in the non-spin-polarized state can also be explained from a chemical bonding point of view. This is facilitated by using the analytical method named crystal orbital Hamilton population (COHP), in which the band structure energy is partitioned into bonding, non-bonding and anti-bonding contributions.[18] As shown in Fig. 3, in the non-spin-polarized case the C–C bond around E_F is in a bonding state, while the C–N one has a strong anti-bonding character. This points to an electronic instability, which can be reduced by adjusting the Fermi level to fill up the bonding states and empty out the anti-bonding ones. For the primitive (1×1) g-C_4N_3, an electronic distortion occurs in which the two spin sublattices become inequivalent. In the spin-polarized state, the bonding character of the C–C bonds is indeed strengthened because the C–C −COHP for the spin-up electrons remains positive and moves below the Fermi level completely. In contrast, the bonding properties of the C–N bonds do not

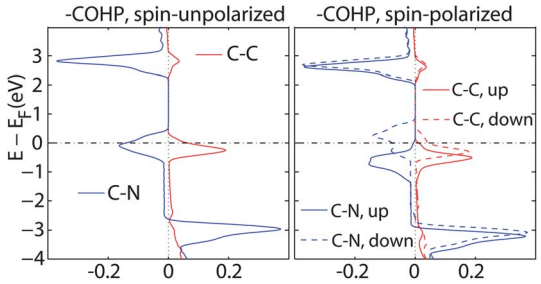

Fig. 3 The −COHP curves for the C–C and C–N bonds of the primitive (1 × 1) g-C_4N_3 cell in both the non-spin-polarized (left) and spin-polarized (right) states. Positive −COHP indicates bonding character, while negative −COHP is for anti-bonding.

change too much, since the C–N −COHP curves remain negative around the Fermi level and move in the opposite direction for the spin-up and spin-down electrons. This is corroborated by the changes of the bond lengths of the C–C and C–N bonds. Although spin polarization shortens the C–C bond length from 1.451 Å to 1.447 Å, the C–N bond lengths only change negligibly (by less than 0.001 Å).

1D g-C_4N_3 nanoribbons

Finally we investigate the effects that edges have on the electronic properties of finite-width 1D g-C_4N_3 nanoribbons. In constructing the model for the g-C_4N_3 nanoribbons, only the connecting C–C bonds are broken, while the *sym*-triazine rings preserve their integrity. As shown in Fig. 4(a) and 5(a), two types of g-C_4N_3 nanoribbons with high-symmetric edge geometries (zigzag and armchair) are constructed and for simplicity edge dangling bonds are passivated with hydrogen. Both zigzag and armchair g-C_4N_3 nanoribbons can be constructed with varying numbers of *sym*-triazine rings, *n*, contained in one unit cell. These are denoted respectively as *n*Z-g-C_4N_3 and *n*A-g-C_4N_3. Our calculations show that both the zigzag and armchair g-C_4N_3 nanoribbons with the narrowest width are spin-polarized semiconductors, with the band gap of the spin-up channel being much larger than that of the spin-down channel. As the ribbon width is increased, the spin-up channel of both zigzag and armchair nanoribbons with H-terminated edges remains semiconducting with a band gap larger than 2.0 eV, whereas that of the spin-down channel shrinks until an energy band eventually crosses E_F, *i.e.* until the ribbon becomes a quasi-1D half-metal. The critical widths for the zigzag and armchair ribbons to be half-metals are calculated to be 19.42 Å (5Z-g-C_4N_3) and 28.86 Å (12A-g-C_4N_3), respectively.

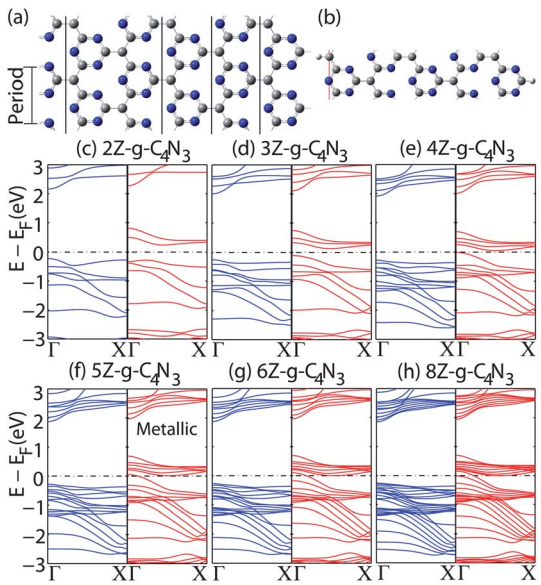

Fig. 4 (a) Schematic of the zigzag g-C_4N_3 nanoribbons with different widths, (b) optimized atomic structure of the H-terminated 5Z-g-C_4N_3 in one unit cell, and the spin-resolved band structures of H-terminated zigzag g-C_4N_3 nanoribbons with different widths are plotted in panels (c)–(h).

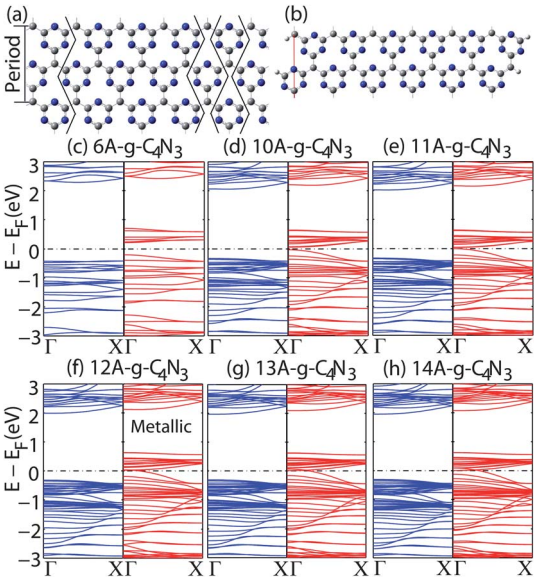

Fig. 5 (a) Schematic of the armchair g-C_4N_3 nanoribbons with different widths, (b) optimized atomic structure of H-terminated 12A-g-C_4N_3 in a unit cell (b), and the spin-resolved band structures of H-terminated armchair g-C_4N_3 nanoribbons with different widths are plotted in panels (c)–(h).

Just like for graphene nanoribbons,[19] also here H represents only a convenient strategy for passivating the edge dangling bonds but other functional groups, such as methyl (–CH_3) and amine (–NH_2), can be used. The replacement of the passivating hydrogen atoms with the methyl group has only a minor influence on the electronic properties of zigzag and armchair g-C_4N_3 nanoribbons: g-C_4N_3 nanoribbons with a narrow width are still spin-polarized semiconductors and then they become half-metals when their width is large enough (see ESI Fig. S2†). The critical width for the occurrence of the transition from a magnetic semiconductor to a half-metal remains unchanged for zigzag ribbons (5Z-g-C_4N_3) but becomes slightly smaller for armchair ribbons (11A-g-C_4N_3). This is not a surprising result, since the methyl group is a σ-type functional group[20] and cannot efficiently couple to the electronic states of the g-C_4N_3 nanoribbons around E_F. In contrast, when two amine groups are used to passivate the dangling bonds at both edges

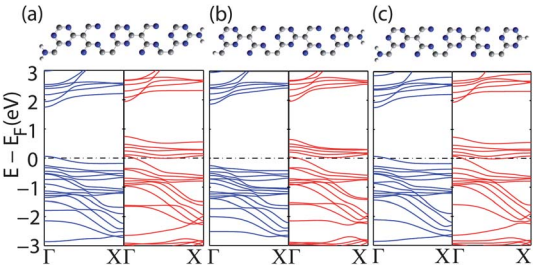

Fig. 6 Optimized atomic structures and the corresponding spin-resolved band structures of 5Z-g-C_4N_3 with the two dangling bonds passivated by amine groups (a), only the dangling bond at the *sym*-triazine ring passivated by an amine group (b) and only the dangling bond at the connecting carbon atom passivated by an amine group. In (b) and (c) the other dangling bond at the opposite edge is passivated with one hydrogen atom.

of a *n*Z-g-C_4N_3 nanoribbon, a dramatic change occurs: the spin-up channel becomes metallic regardless of the ribbon width and thus the half-metallic ground state is destroyed completely. Fig. 6(a) shows a typical result for the 5Z-g-C_4N_3 nanoribbon.

In order to obtain a deeper insight into this feature, we investigate two more structures constructed from the 5Z-g-C_4N_3 nanoribbon, in which only the dangling bond either at the connecting C atom or at the carbon atom in the *sym*-triazine ring is passivated with an amine group and the other dangling bond at the opposite edge is still passivated with H (Fig. 6b and c). We find that the amine group bonded to C in the *sym*-triazine ring hardly modifies the band structure of the ribbon, whereas the one bonded to the connecting C pushes one spin-up energy band across the Fermi level and makes the spin-up channel metallic. A similar feature is also observed in armchair g-C_4N_3 nanoribbons. In amine, when a nitrogen atom interacts with the other three atoms or with functional groups, four asymmetrical sp^3 hybridized orbitals are formed. Three of them create three corresponding σ-type bonds, while the remaining one is occupied by the N lone pair. Just like for 1,4-diaminobenzene molecules,[21,22] the sp^3-orbital occupied by the lone pair is electronically very different from the other three, since it is basically p-type. Therefore, when an amine group is bonded directly to a connecting carbon atom, its lone pair can interact strongly with the C $2p_z$ orbital so as to modify the band structure of the ribbon. This not only shows the critical role of the connecting carbon atom in the electronic properties of g-C_4N_3 but also demonstrates an efficient way to tailor the electronic properties of g-C_4N_3 nanoribbons.

4 Conclusion

We have investigated the electronic and magnetic properties of g-C_4N_3 in different dimensions by using DFT calculations, and found that the $2p_z$ orbital of the carbon atom connecting the *sym*-triazine units plays a decisive role in their half-metallic characteristics. In 2D bulk g-C_4N_3 sheets, such $2p_z$ orbital couples weakly with the frontier molecular orbitals of the *sym*-triazine ring due to either symmetry mismatch or the large energy separation. As a consequence it forms a narrow energy band near the Fermi level and favors a parallel spin orientation, thereby giving rise to spin polarization in the (1×1) primitive cell. The (2×2) reconstruction then enhances the half-metallic characteristics of the 2D g-C_4N_3 sheet. When dimensions are reduced, finite-size and edge effects become dominant. Both zigzag and armchair g-C_4N_3 nanoribbons with H-terminated edges remain half-metallic for widths larger than a critical value, otherwise they are spin-polarized semiconductors. The electronic and magnetic properties of these g-C_4N_3 nanoribbons can be tuned further by adjusting the interaction between the passivating group and the $2p_z$ orbital of the connecting C atom at the ribbon edges. Our findings indicate a strategy for tuning the magnetic properties of this intriguing class of p-type magnets towards applications in future spintronic devices.

Acknowledgements

This project is supported by the National Natural Science Foundation of China (no. 61071012 and 61271050) and the MOST of China (no. 2011CB933001 and 2013CB933404). SS is grateful for additional funding support from Science Foundation of Ireland (grant no. 07/IN/I945) and by CRANN.

References

1 M. I. Katsnelson, V. Yu. Irkin, L. Chioncel, A. I. Lichtenstein and R. A. de Groot, *Rev. Mod. Phys.*, 2008, **80**, 315.
2 J. M. D. Coey and S. Sanvito, *J. Phys. D: Appl. Phys.*, 2004, **37**, 988.
3 J.-H. Park, E. Vescovo, H.-J. Kim, C. Kwon, R. Ramesh and T. Venkatesan, *Nature*, 1998, **392**, 794.
4 R. A. de Groot, F. M. Mueller, P. G. van Engen and K. H. J. Buschow, *Phys. Rev. Lett.*, 1983, **50**, 2024.
5 J. E. Medvedeva, A. J. Freeman, X. Y. Cui, C. Stampfl and N. Newman, *Phys. Rev. Lett.*, 2005, **94**, 146602.
6 B. Dlubak, M.-B. Martin, C. Deranlot, B. Servet, S. Xavier, R. Mattana, M. Sprinkle, C. Berger, W. A. De Heer, F. Petroff, A. Anane, P. Seneor and A. Fert, *Nat. Phys.*, 2012, **8**, 557.
7 C. Biswas and Y. H. Lee, *Adv. Funct. Mater.*, 2011, **21**, 3806.
8 Y. W. Son, M. L. Cohen and S. G. Louie, *Nature*, 2006, **444**, 347.
9 E. Kan, Z. Li, J. Yang and J. G. Hou, *J. Am. Chem. Soc.*, 2008, **130**, 4224.
10 J. S. Lee, X. Q. Wang, H. M. Luo and S. Dai, *Adv. Mater.*, 2010, **22**, 1004.
11 A. Du, S. Sanvito and S. C. Smith, *Phys. Rev. Lett.*, 2012, **108**, 197207.
12 J. M. Soler, E. Artacho, J. D. Gale, A. García, J. Junquera, P. Ordejón and D. Sánchez-Portal, *J. Phys.: Condens. Matter*, 2002, **14**, 2745.
13 N. Troullier and J. Martins, *Phys. Rev. B: Condens. Matter Mater. Phys.*, 1991, **43**, 1993.
14 J. Perdew, K. Burke and M. Ernzerhof, *Phys. Rev. Lett.*, 1996, **77**, 3865.
15 M. J. Frisch, *et al.*, *Gaussian 03, revision B03*, Gaussian Inc., Pittsburg, PA, 2003.

16 M. J. Frisch, J. A. Pople and J. S. Binkley, *J. Chem. Phys.*, 1984, **80**, 3265.
17 W. Pychhout, I. Callaerts, C. van Alsenoy, H. J. Geise, A. Almenningen and R. Seip, *J. Mol. Struct.*, 1986, **147**, 321.
18 R. Dronskowski, *Computational Chemistry of Solid State Materials: A Guide for Materials Scientists, Chemists, Physicists and Others*, Wiley-VCH, Weinheim, 2005.
19 F. Cervantes-Sodi, G. Csányi, S. Piscanec and A. C. Ferrari, *Phys. Rev. B: Condens. Matter Mater. Phys.*, 2008, **77**, 165427.
20 D. J. Mowbray, G. Jones and K. S. Thygesen, *J. Chem. Phys.*, 2008, **128**, 111103.
21 F. A. Carey, *Organic Chemistry*, 2nd edn, McGraw-Hill, New York, 1992.
22 J. Ning, R. Li, X. Shen, Z. Qian, S. Hou, A. R. Rocha and S. Sanvito, *Nanotechnology*, 2007, **18**, 345203.